Dalton Transactions

ROYAL SOCIETY OF CHEMISTRY

PAPER

View Article Online
View Journal | View Issue

Check for updates

Cite this: *Dalton Trans.*, 2021, **50**, 9236

Pseudotetrahedral copper(II)-complexes with enantiopure (*R* or *S*)-2-(((aryl)ethylimino)ethyl) phenolate Schiff base ligands†

Mohammed Enamullah, *[a] Mohammad Anwar Hossain, [a] Mohammad Khairul Islam, [a] Dennis Woschko [b] and Christoph Janiak *[b]

Condensation of 2-hydroxy-benzophenone (HL′) with (*R* or *S*)-(Ar)ethylamine yields the enantiopure Schiff bases (*S* or *R*)-2-((*E*)-1-(1-(Ar)ethylimino)ethyl)phenol {Ar = C_6H_5 (*S*- or *R*-HL^1), *p*-$CH_3OC_6H_4$ (*S*- or *R*-HL^2)}. These Schiff bases react with copper(II) acetate under reflux to give green microcrystals of bis[(*R* or *S*)-2-((*E*)-1-(1-(Ar)ethylimino)ethyl)phenolato-κ^2N,O]-Λ/Δ-copper(II), {Ar = C_6H_5 (Λ/Δ-Cu-*R*- or *S*-L^1), *p*-$CH_3OC_6H_4$ (Λ/Δ-Cu-*R*- or *S*-L^2)} with induction of Λ/Δ-chirality at-metal. The presence of Schiff base ligands in the paramagnetic green microcrystals is confirmed by decomplexation reaction with NaCN *via* reduction of Cu(II) to Cu(I) in DMSO-d_6 solution. Crystallization attempts of the green microcrystalline Schiff-base Cu complexes provide deep-green block-shaped crystals of an about equal admixture of bis[2-oxo-benzophenonato-κ^2O,O′]-copper(II), (CuL′$_2$) and bis[2-(imino(phenyl)methyl)phenolato-κ^2N,O] copper(II), (CuL″$_2$) *via in situ* hydrolysis of the coordinated Schiff base ligands back to 2-hydroxy-benzophenone (HL′) and to 2-(imino(phenyl)methyl)phenol (HL″), which in-turn bind with the copper(II) ion. Powder X-ray diffraction (PXRD) patterns of *R*-HL^1 and Cu-*R*-L^1 allowed their structure determinations using the program Expo-2014 followed by Rietveld refinement. The Cu structures refined to four-co-ordinated Λ/Δ-copper(II)-complexes by the two phenolate-oxygen and two imine-nitrogen atoms from two Schiff base ligands in a pseudotetrahedral geometry. DFT optimized structures (at gas-phase) reveal the Δ-Cu-*S*-L^1 or Λ-Cu-*R*-L^1 diastereomer as slightly more stable than the corresponding Λ-Cu-*S*-L^1 or Δ-Cu-*R*-L^1 by *ca.* 7.60 kcal mol^{-1}, resulting from diastereoselectively induced Λ *vs.* Δ-chirality at-metal. Electronic circular dichroism (ECD) spectra display mirror-image relationships and comparisons of experimental and simulated ECD spectra by TDDFT suggest an excess of the Δ-Cu-*S*-L^1 or Λ-Cu-*R*-L^1 diastereomer in solution. The cyclic voltammograms demonstrate two one electron charge transfer processes for Cu^{2+}/Cu^+ and Cu^+/Cu^0 couples in acetonitrile, respectively.

Received 23rd May 2021,
Accepted 8th June 2021

DOI: 10.1039/d1dt01671g

rsc.li/dalton

Introduction

Chiral/achiral bidentate N,O-chelate Schiff base ligands can provide four coordinated non-planar C_2-symmetrical transition metal(II)-complexes with tetrahedral or pseudotetrahedral geometry with Fe(II), Co(II), Ni(II), Cu(II) and Zn(II). The molecular structures of these complexes are of continued interest in the context of the *chiroptical* properties, metal-centred induced Λ *vs.* Δ-chirality and concomitant (dia)stereoselectivity.[1,2] With enantiopure *R*- or *S*-N,O chelate ligands, an induced chirality at-metal adds right (Δ)- and left (Λ)-handed helical isomers and can give two opposite configured diastereomers Δ-M(*R*-N,O)$_2$ and Λ-M(*R*-N,O)$_2$ {or Λ-M(*S*-N,O)$_2$ and Δ-M(*S*-N,O)$_2$} whose relative amount can be different in solution and in the solid state (Scheme 1).[3–14]

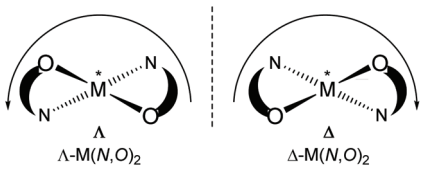

Scheme 1 Enantiomeric configurations at the metal of a non-planar bis-N,O-chelate complex viewed along the C_2 axis (perpendicular to the paper plane): Λ left-handed helicity, Δ right-handed helicity along the C_2 axis.

[a]*Department of Chemistry, Jahangirnagar University, Dhaka-1342, Bangladesh. E-mail: enamullah@juniv.edu*
[b]*Institut für Anorganische Chemie und Strukturchemie, Heinrich-Heine-Universität, Universitätsstr. 1, D-40225 Düsseldorf, Germany. E-mail: janiak@uni-duesseldorf.de*

†Electronic supplementary information (ESI) available: Optimized structures, IR-spectra, simulated UV-Vis/CD spectra, PXRD data, CV data, cif/checkcif files and excited state properties. CCDC 2060528 for *R*-HL^1 and 2060529 for CuL′$_2$/CuL″$_2$. For ESI and crystallographic data in CIF or other electronic format, see DOI: 10.1039/d1dt01671g

The non-covalent inter- and intra-complex interactions and the interactions to the solvent molecules in solution result in free energy differences between the two diastereomers, leading to one of the diastereomers being thermodynamically favoured. In this connection, ligand chirality and design, substituents, steric constraints, metal ion and counter anion selection, solute-solvent interactions, reaction environment, crystallization protocol, pH of solution and redox reactions can significantly control the phenomenon.[3–14]

Concerning the chirality induction at-metal and thereby diastereoselection in $M(N,O)_2$ complexes with N,O = chiral bidentate salicylaldiminate (Schiff base) ligand the crucial question is the diastereomeric purity. Typically, solid-state single-crystal structures (from one crystal) are taken as the basis to assign the diastereomer as Δ-M(*R*-N,O)$_2$ or Λ-M(*R*-N,O)$_2$, *etc*. This does not rule out that already the single crystal batch may form a mixture of diastereomers and that the preferred diastereomer may be different in solution, including diastereomer equilibria with Λ/Δ-helicity inversion.[3,4,9a] Enantiopure salicylaldimine ligands can give single diastereomers in one crystal, but the solution diastereoselection can be very poor. This was addressed by Scott *et al.* for the solid state by matching simulated and experimental powder X-ray data under the assumption that the other diastereomer will have an independent crystal structure and display a distinctly different powder X-ray diffraction pattern.[9b]

Solid-state *versus* solution studies with X-ray, vibrational circular dichroism and NMR along with theoretical calculations revealed that diastereoselection is phase dependent for the explored solvation-induced helicity inversion at-metal from Λ-Cu-*R* or Δ-Cu-*S* at solid-state to Δ-Cu-*R* or Λ-Cu-*S* in solution for Schiff base complexes.[3,15] Solvent dependent helicity inversion from Δ-Ni (in acetonitrile) to Λ-Ni (in DMSO) was reported in tris(diamine)nickel(II), whereas both stereoisomers coexist with almost equal ratio at the solid-state.[13a] Similarly, variation of pH of the solution or solvent polarity led to an epimerization of metal centred chirality in Ti(IV)/Re(I)-complexes.[13b,c] Indeed, certain redox-reactions led to changes in the chirality at-metal in Co/Cu(II)-chiral-ligand complexes.[14]

Our recent works along induced chirality at-metal and diastereoselection showed a phase-dependent preferred formation of the Δ-M or Λ-M diastereomer in non-planar or pseudotetrahedral mononuclear [M(*R* or *S*-N,O)$_2$] (M = Fe, Co, Ni, Cu, Zn and N,O$^-$ = salicylaldiminato/oxo-naphthaldiminato ligands[16]), examined by X-ray, ^{1}H NMR-/ECD-/VCD-spectroscopy, DSC and DFT/TDDFT.[3–8,15] X-ray structure determinations, the most reliable method to assign the absolute configuration in the solid state, reveal that coordination of *R*- or *S*-N,O ligands to the metal ions typically gives Λ-M-*R* or Δ-M-*S* as major diastereomer in an investigated enantiopure single crystal (not ruling out the co-existence of crystals of the other diastereomer in the batch).[3–8,15] Only in a few cases, both diastereomers co-exist in a single crystal.[1i,5] In solution, a dynamic equilibrium between two diastereomers can lead to Λ/Δ-helicity inversion, as shown by variable time and/or temperature ^{1}H NMR and ECD spectra.[3b,4,7a,8a]

Synthesis of Schiff base ligands is a reversible process, and hydrolysis shifts the equilibrium to the reverse direction with reformation of the aldehyde or ketone and the amine.[17] The *in situ* hydrolysis of a Schiff base during complexation and/or a slow crystallization process, due to presence of small amounts of water, has been described before.[17,18] The hydrolytic cleavage of the imine-bond in the presence of a metal ion or in the (coordinated) Schiff base can then lead to the formation of the metal(II)-aldehydate or -ketonate complexes.[17b,18d] We have recently reported two cases of *in situ* hydrolysis of Schiff base ligands during the complexation and/or crystallization process with a copper(II)-salt, which provided mononuclear bis[salicylaldehydato-κ^{2}O,O′]copper(II)[19] and bis[2-oxo-1-naphthaldehydato-κ^{2}O,O′]copper(II)[19b] and dinuclear (μ-salicylaldehydato)(2,2′-bipyridine)(nitrato)-copper(II).[19a]

The present paper reports the results of the synthesis and spectroscopic characterization of the enantiopure Schiff base ligands (*S* or *R*)-2-((*E*)-1-(1-(Ar)ethylimino)ethyl)phenol (*S*- or *R*-HL) and their complexes bis[(*R* or *S*)-2-((*E*)-1-(1-(Ar)ethylimino)ethyl)phenolato-κ^{2}N,O]-Λ/Δ-copper(II), [Λ/Δ-Cu-*S*- or *R*-L]. Crystallization of these complexes failed and only the *in situ* hydrolysis products could be obtained as an almost equal admixture of bis[2-oxo-benzophenonato-κ^{2}O,O′]-copper(II), (CuL′$_2$) and bis[2-(imino(phenyl)methyl)phenolato-κ^{2}O,N], (CuL″$_2$) (Scheme 2). For the diastereoselection of Λ/Δ-Cu-*S*- or *R*-L a combination of experimental (UV-Vis and ECD) and computational procedures including structure optimizations and excited state properties by DFT/TDDFT is employed to assess the chirality induction at-metal. In addition, solid state X-ray and PXRD measurements are carried out to elucidate the molecular structures of the ligands and the complexes.

Results and discussion

The enantiopure Schiff base ligands (*S* or *R*)-2-((*E*)-1-(1-(Ar)ethylimino)ethyl)phenol {*S*- or *R*-HL: Ar = C_6H_5 (*S*- or *R*-HL^1) and *p*-$CH_3OC_6H_4$ (*S*- or *R*-HL^2)} were synthesized from the reaction between 2-hydroxy-benzophenone (HL′) and an enantiopure amine (*R* or *S*)-(Ar)ethylamine (Scheme 2). These Schiff base ligands react with copper(II) acetate under reflux to provide deep-green microcrystals of bis[(*R* or *S*)-2-((*E*)-1-(1-(Ar)ethylimino)ethyl)phenolato-κ^{2}N,O]-Λ/Δ-copper(II), (Λ/Δ-Cu-*R*- or *S*-L) {Ar = C_6H_5 (Λ/Δ-Cu-*R*- or *S*-L^1) and *p*-$CH_3OC_6H_4$ (Λ/Δ-Cu-*R*- or -*S*-L^2)}.

Surprisingly, from single-crystal X-ray diffraction the deep-green block-shaped crystal product of the complex Cu-*R*-L^1 is analyzed as bis[2-oxo-benzophenonato-κ^{2}O,O′]-copper(II), (CuL′$_2$) in an about equimolar mixture with bis[2-(imino(phenyl)methyl)phenolato-κ^{2}N,O]copper(II), (CuL″$_2$) (Scheme 2). As the formation of the Schiff base ligands and their purity had been established by various methods, obviously an *in situ* hydrolysis of the (coordinated) Schiff base ligands had occurred during the slow crystallization process due to the presence of a small amount of water in the sample.[17–19]

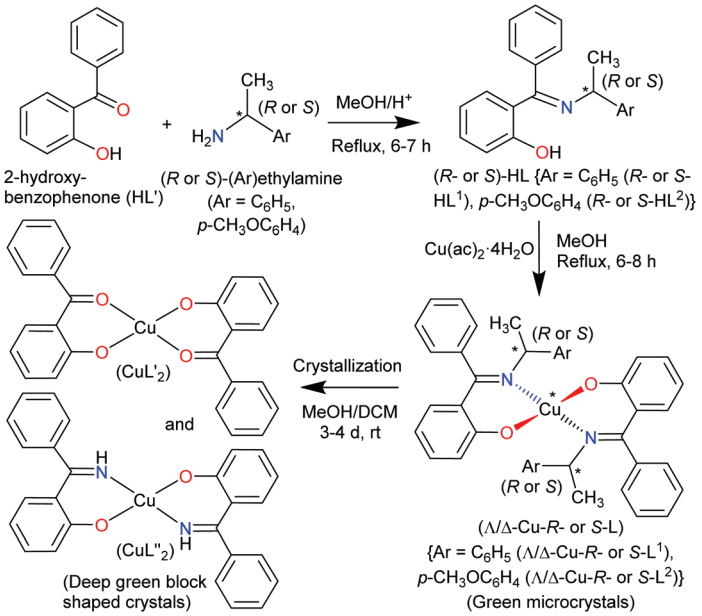

Scheme 2 Synthetic route to the formation of the copper(II)-complexes.

The reaction for the normal hydrolysis of a Schiff base ligand, opposite to its formation, is as given in eqn (1) and is initiated by a nucleophilic attack of water on the imine carbon atom.

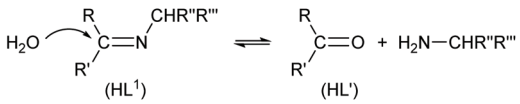

(1)

Remarkably, here the *in situ* hydrolysis had not only occurred along the Ar(Ph)C=N(alkyl) bond with re-formation of the starting 2-hydroxy-benzophenone (HL′) but also along the N–C(alkyl) bond with formation of 2-(imino(phenyl) methyl)phenol (HL″). Our results show that apparently for a (Cu-coordinated) imine nitrogen atom, the direction of hydrolysis cannot only occur at the C=N bond but also along the N–C(alkyl) bond. The latter leads to an imine and alcohol according to eqn (2) and is initiated by the nucleophilic attack of water on the N-bound alkyl carbon atom. The substitution of two aryl groups on the imine-carbon atom with their steric shielding in the case of L^1 may facilitate the nucleophilic attack of water on the N-bound alkyl carbon atom. Following the nucleophilic attacks of H_2O, subsequent proton shifts to the imine-N atom then cleave the respective C=N or N–C bonds.

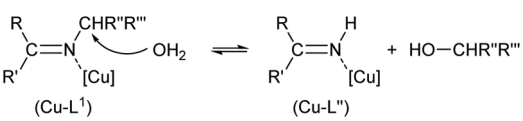

(2)

Both deprotonated ligands L'^- and L''^- then coordinate to copper and form bis-chelate ligands complexes. Both homoleptic complexes CuL'_2 and CuL''_2 crystallized as a mixture sharing the same crystallographic position. Alternatively, a mixed-ligand complex CuL′L″ could have formed (which would then show a ligand disorder on the centrosymmetrical site). As the Cu atom sits on an inversion symmetry site this renders the two ligands symmetry equivalent and the two possibilities cannot be differentiated by crystallography. Also, a mixed crystal of CuL′L″ with some $Cu(L')_2$ is possible, as crystallographically the shared keto O and imine N atoms refine to a ratio of 56/44. Spectroscopy confirms the presence of the imine in the crystal product. IR spectra show the main characteristic bands of νC=N at *ca.* 1605 cm^{-1} in Schiff base ligands (*R*- or *S*-HL) (Fig. S6a, ESI†) and *ca.* 1607 cm^{-1} in green microcrystals (Cu-*R* or *S*-L) (Fig. S6b, ESI†). Spectra for the deep-green block-shaped crystals (admixture of CuL'_2 and CuL''_2) show peaks at *ca.* 3325 cm^{-1} (νN–H) and *ca.* 1601/1579 cm^{-1} (νC=N/O) (Fig. S6c, ESI†). Calculated IR spectra from optimized structures of CuL'_2 or CuL''_2 by DFT at the b3lyp/6-31 g(d) level exhibit these bands at a comparable range (Fig. S6d, ESI† and see Experimental section). In electron impact (EI) mass spectra, the deep-green block-shaped crystal sample obtained from the crystallization of Cu-*R* or *S*-L^1 show the ion peaks of the hydrolysis products at m/z = 198 for $[HL']^+$, 197 $[HL'']^+$ and 196 $[HL''–H]^+$. The complex molecular ion peaks are at m/z = 457 $[CuL'_2]^+$, 456 $[CuL'_2–H$ or Cu-L′L″$]^+$ and 455 $[CuL''_2]^+$ (Fig. S7, ESI†). The mass spectra give further ion peaks at m/z = 260 for $[CuL']^+$, 258 for $[CuL''–H]^+$, 121 for $[\{(C_6H_4OH)CHO\}–H]^+$ and 105 for $[\{C_6H_5CHO\}–H]^+$.

^{1}H-NMR spectra

^{1}H NMR spectra for Schiff base ligands show a doublet at δ 1.53–1.57 ppm (J_{HH} = 6.8 Hz) for the methyl protons and a quartet at δ 4.49–4.55 ppm (J_{HH} = 6.8 Hz) for the methine proton (Fig. 1).[16] In addition, the spectra show a sharp singlet at δ 3.82 ppm for the *p*-methoxy protons in *R*- or *S*-HL^2. The

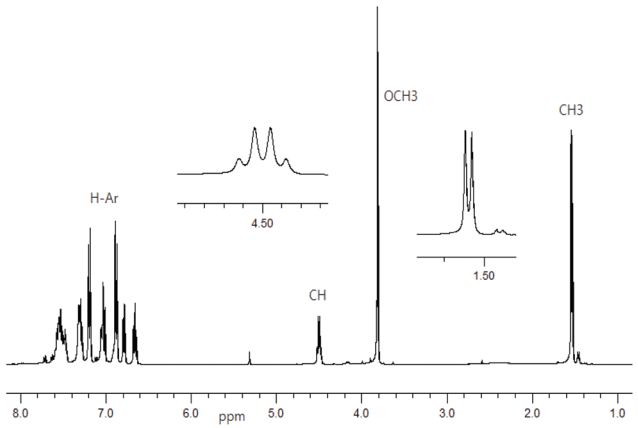

Fig. 1 ^{1}H NMR spectrum for *R*-HL^2 in $CDCl_3$ at 20 °C.

spectra are dominated by several peaks as doublet, triplet, doublet of doublet, doublet of triplet and multiplet at δ 6.66–6.71 ppm for the aromatic protons (see Experimental section). The presence of the *p*-methoxy group as substituent on the aryl-ring in *R*- or *S*-HL^2 shifts the methine proton signal upfield by *ca.* 0.05 ppm in contrast to that in *R*- or *S*-HL^1 due to an electron inductive effect. However, the signal for the phenolic proton (acidic) could not be detected in $CDCl_3$ solution.

Decomplexation reaction of Cu-*R*-L^1 with NaCN

To check the formation of paramagnetic Cu-*R*-L, that is, to verify the presence of the intact Schiff base ligand (HL) in the green microcrystals (Scheme 2) by ^{1}H NMR, we employed a decomplexation reaction of Cu-*R*-L^1 with NaCN with concomitant reduction of Cu(II) to Cu(I) in DMSO-d_6 solution.[5,6,8b] The reaction results in the formation of diamagnetic $[Cu^I(CN)_4]^{3-}$ and free Schiff base (*R*-HL^1) in solution, accompanied by a colour change from deep-green to light-orange. The ^{1}H NMR spectrum of this solution (Fig. 2) is identical to the neat Schiff base (Fig. 1) and shows a doublet at δ 1.47 ppm (J_{HH} = 6.4 Hz) for the methyl protons and a quartet at δ 4.45 ppm (J_{HH} = 6.2 Hz) for the methine proton. The phenolic proton appears as a broad signal at δ 15.55 ppm. Indeed, there is no peak which corresponds to the hydrolyzed ligands 2-hydroxy-benzophenone (HL′) and/or 2-(imino(phenyl)methyl)phenol (HL″). This result suggests the formation of the Cu-*R*- or *S*-L complexes which provide bis[2-oxo-benzophenonato-κ^{2}O,O′]-copper(II), (CuL′$_2$) and bis[2-(imino(phenyl)methyl)phenolato-κ^{2}N,O] copper(II), (CuL″$_2$) *via in situ* hydrolysis of the coordinated Schiff base during the subsequent crystallization in MeOH/DCM (Scheme 2).

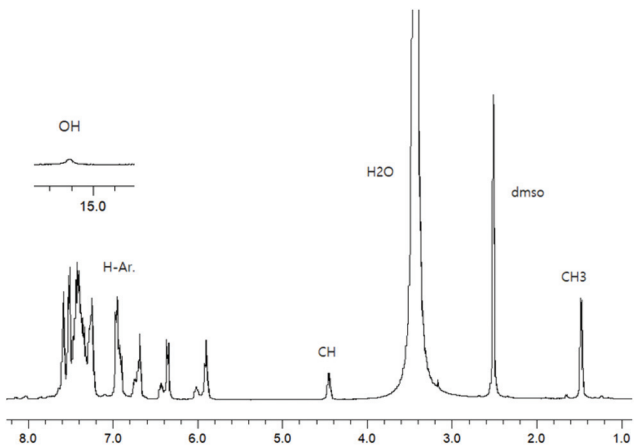

Fig. 2 ^{1}H NMR spectrum from the decomplexation reaction of Cu-*R*-L^1 with NaCN in DMSO-d_6 at 20 °C.

X-ray structures for *R*-HL^1, CuL′$_2$ and CuL″$_2$

The molecular structure for *R*-HL^1 is shown in Fig. 3 and selected bond lengths and angles are listed in Table 1. *R*-HL^1 crystallizes in the monoclinic space group $P2_1$. The refinement for an absolute structure with a Flack parameter of 0.04(7) (*cf.* Table 4) indicates that the investigated crystal is enantiopure. A Flack parameter close to zero confirms the absolute structure of the crystal and excludes the presence of the Schiff base molecule with *S*-chirality at C14. The N1–C7 bond length of 1.288(2) Å indicates the double bond character of the imine,

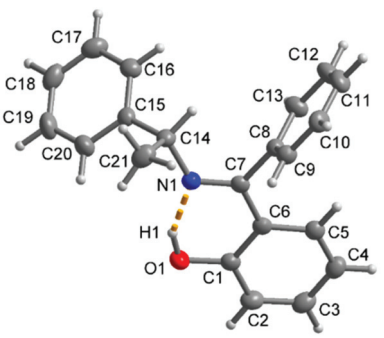

Fig. 3 Molecular structure of *R*-HL^1 with the dashed orange line showing the intramolecular hydrogen bond with O1–H1 0.91(2) Å, H1···N1 1.70(3) Å, O1···N1 2.533(2) Å, O1–H1···N1 angle 151(2)°.

Table 1 Selected bond lengths (Å) and angles (°) in *R*-HL^1, CuL′$_2$ and CuL″$_2$

Bond lengths (Å)/angles (°)	*R*-HL^1	CuL′$_2$	CuL″$_2$
Cu–O1		1.9070(16)	1.9070(16)
Cu–O2		1.89(1)	—
Cu–N1		—	1.96(2)
O1–C1	1.347(2)	1.308(3)	
N1/O2–C7	1.288(2)	1.25(11)	1.34(2)
N1–C14	1.470(2)	—	
C6–C7	1.473(2)	1.446(3)	
C7–N1–C14	121.73(13)	—	
C1–O1–H1	106.2(14)	—	
C6–C7–N1	118.18(1)		
O1–Cu–O2	—	90.1(3)	—
O1–Cu–N1	—		95.1(5)
O1–Cu–O2^i/N1^i	—	89.9(3)	84.9(5)

Symmetry transformation i = $-x$ + 1, $-y$ + 2, $-z$ + 1.

while the C7–N1–C14 bonding angle of 121.73(13)° represents a sp^2-hybridization of the imino-nitrogen atom. There is an intramolecular hydrogen bond from the phenol (O-)H atom to the imine N atom.

The molecular structure for CuL'_2 and CuL''_2 on their shared centrosymmetry position is depicted in Fig. 4. For clarity also the individual CuL'_2 and CuL''_2 complexes are shown. Both complexes are square-planar. The Cu atom occupies the crystallographic inversion center so that both ligands are symmetry equivalent. The bond lengths are largely as expected. We note that the imino-N atom could only be refined isotropically. Crystallographically the shared position of the two complexes manifests itself as disorder of the keto-O and imino-N atom which refined to 56/44 occupancy. The disorder then led to a lower accuracy in the involved C–O, C–N and Cu–O, Cu–N bond distances (Table 1).

PXRD-derived structures for *R*-HL^1 and Cu-*R*-L^1

Because of the failure to grow single crystals of Cu-*S*- or *R*-L^1 in X-ray quality due to the *in situ* hydrolysis, it was inevitable to determine their structures through powder X-ray diffraction (PXRD) on the green microcrystals of Cu-*S*- or *R*-L^1. PXRD patterns for the Schiff base ligand (*R*-HL^1) and complex (Cu-*R*-L^1) are shown in Fig. 5a, which reveal two distinct phases and hence confirm the formation of the complex. PXRD patterns reflect a well-defined crystalline nature and allowed for structure determination using the program Expo-2014[20] followed by Rietveld refinement.[21–23] For structure solution calculations, we used the gas-phase optimized structures for *R*-HL^1 and Cu-*R*-L^1 (both Λ-Cu and Δ-Cu diastereomers, see below) as input files, respectively. The experimental and calculated Rietveld refinement plots are in good agreement with very little difference (Fig. 5b, Fig. S8, and S9, ESI†). The structure for Cu-*R*-L^1 reveals that two phenolate-oxygen and two imine-nitrogen atoms from two molecules of Schiff base ligands form a non-planar N_2O_2-coordination sphere around copper(II) in a pseudotetrahedral geometry (Fig. 6a and b). The structure solved for *R*-HL^1 (Fig. 6c) is very similar to its single crystal X-ray structure (Fig. 2), discussed above. The selected bond lengths

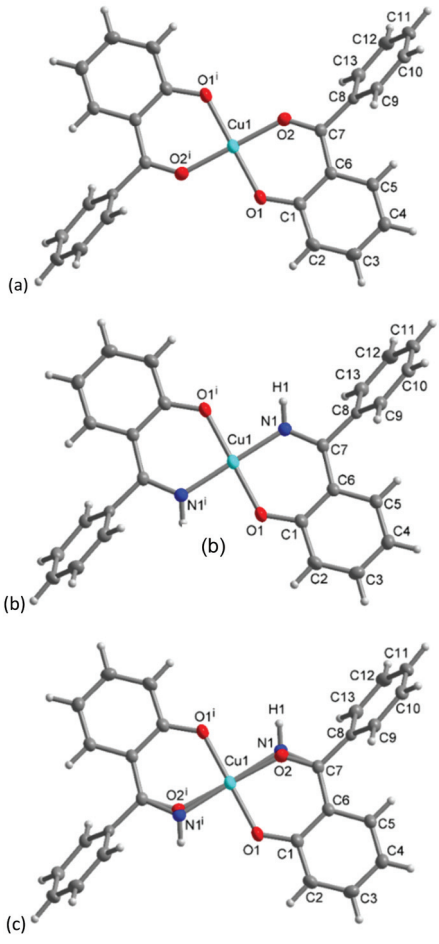

Fig. 4 Molecular structures of (a) CuL'_2 and (b) CuL''_2 shown individually and (c) on their shared crystallographic site. Selected bond lengths and angles are given in Table 1. Symmetry transformation $i = -x + 1, -y + 2, -z + 1$.

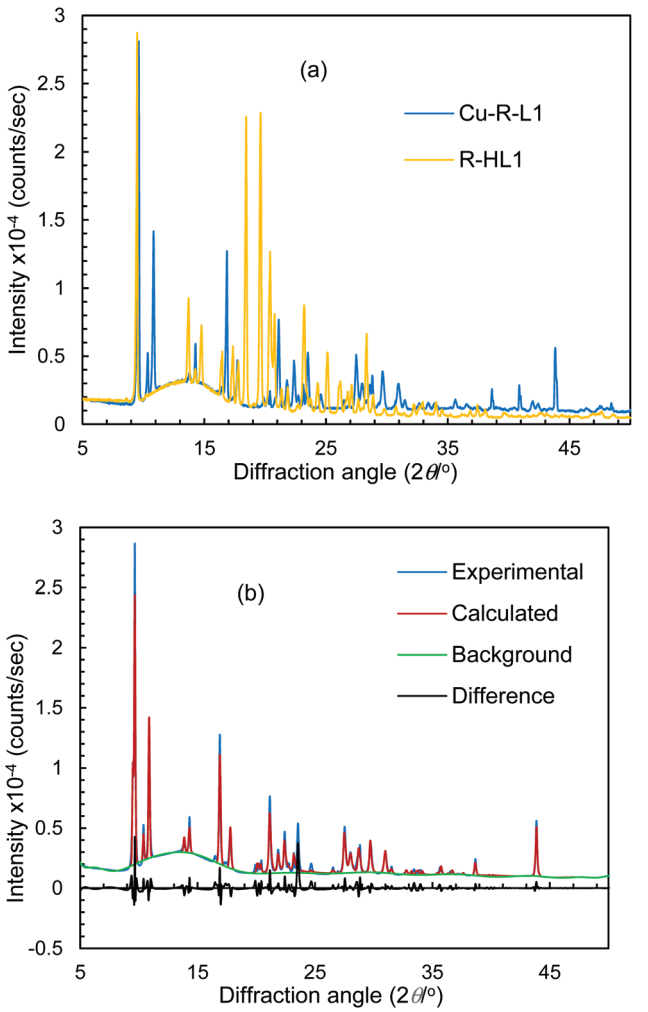

Fig. 5 (a) PXRD patterns for *R*-HL^1 and Cu-*R*-L^1. (b) Experimental and calculated Rietveld refinement plots for Cu-*R*-L^1 (calculated for Λ-Cu-*R*-L^1; see Fig. S8, S9, ESI† for *R*-HL^1 and Δ-Cu-*R*-L^1).

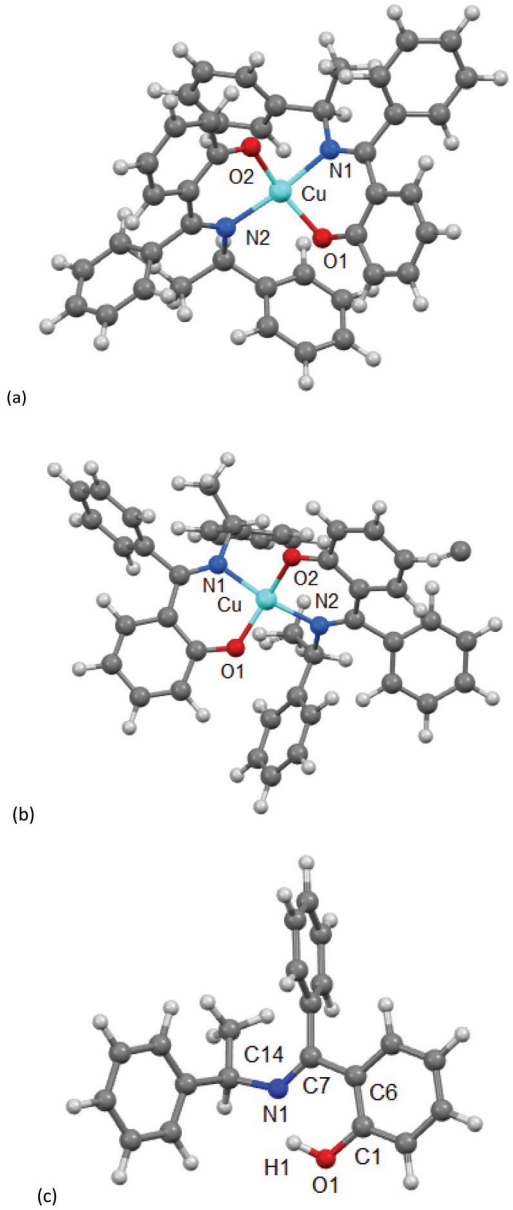

Fig. 6 PXRD-derived structures for (a) Λ-Cu-*R*-L^1, (b) Δ-Cu-*R*-L^1 (b) and (c) *R*-HL^1.

and angles in *R*-HL^1 and Cu-*R*-L^1 are listed in Table 2, very close to the X-ray results for *R*-HL^1 (Table 1) and for an analogous Δ-Cu-*R*-L complex[3a] (Table 2). In fact, PXRD structures satisfy well to both diastereomers of Λ-Cu-*R*-L^1 and Δ-Cu-*R*-L^1 and obviously cannot determine the absolute configuration of the metal ion (*e.g.*, Λ-Cu or Δ-Cu) as in case of a single-crystal X-ray structure.

For analyses of coordination geometry of Λ/Δ-Cu-*R*-L^1, we measured the degree of distortion from tetrahedral to square-planar based on the dihedral angle θ/° (*i.e.*, angle between two coordinating O1–Cu–N1 and O2–Cu–N2 planes) and its normalized function $\tau_{tet\text{-}sq}(\theta/90°)$.[3–8,15] The values of θ are 0° (or $\tau_{tet\text{-}sq}$ = 0) for square-planar and 90° (or 1.0) for tetrahedral geometry (not considering the inherent distortion induced by the chelate ring formation). The values are found to be 33.6° (θ)/0.37 ($\tau_{tet\text{-}sq}$) for Λ-Cu-*R*-L^1 and 40.2°/0.45 for Δ-Cu-*R*-L^1, which are comparable to literature values for the analogous bis[(*R*)-*N*-1-(phenyl)ethyl-salicylaldiminato]-Δ-copper(II) (42.1°/0.47[3a]) and suggest a pseudotetrahedral geometry around the copper(II) ion.

Electronic spectra (UV-Vis and ECD)

The electronic spectra (UV-Vis) for the green microcrystals Cu-*R*-L^1 or Cu-*S*-L^1 are identical, and comparable to that for the deep-green block-shaped crystals (CuL'_2/CuL''_2) in chloroform. The spectra feature a very strong band below *ca.* 320 nm (λ_{max}/ε_{max} = 260 nm/23 925 L mol^{-1} dm^{-3} for Cu-*R*-L^1 and 265 nm/22 100 L mol^{-1} dm^{-3} for CuL'_2/CuL''_2), assigned to the intra-ligand $\pi \rightarrow \pi^*$/$n \rightarrow \pi^*$ transitions (LL) (Fig. 7). A medium broad band at 320–450 nm (λ_{max}/ε_{max} = 342 nm/5963 L mol^{-1} dm^{-3} for Cu-*R*-L^1 and 349 nm/6250 L mol^{-1} dm^{-3} for CuL'_2/CuL''_2), attributes to the metal–ligand (ML) charge transfer transitions. The spectra further show a very weak broad band at visible region 500–1100 nm (λ_{max}/ε_{max} *ca.* 650 nm/100 L mol^{-1} dm^{-3}), due to the metal-centred d–d (MM) transitions for the copper (II)-core electrons (Fig. 7, inset).[5,7b,24,25,26] The computed UV-Vis spectra by TDDFT, calculated at the m06/sdd//b3lyp/6-31 g(d) level with polarization continuum model (PCM) in chloroform, are shown in Fig. 7, which are very similar to the experimental spectra in solution.

The electronic circular dichroism (ECD) spectra in chloroform exhibit mirror-image relationships for Cu-*R*-L^1 and Cu-*S*-L^1 (Fig. 8). The spectra feature several bands with opposite Cotton effect, associated to the different electronic transitions as observed in the UV-Vis spectra. Indeed, the mirror-image relationships reflect diastereomeric excess of the *S*- or *R*-ligated complexes in solution. The ECD spectral data for Cu-*R*-L^1/Cu-*S*-L^1 are characterized with the band maxima and patterns (sign and strength) at *ca.* 710 nm (±, weak), 570 nm (±, weak), 390 nm (±, medium) and 320 nm (±, strong), respectively. Similar ECD spectral patterns were reported for the analogous transition metal(II)-complexes with *chiral*-N,O-chelate Schiff base ligands in solution (M = Fe, Co, Ni, Cu, Zn).[3,4,5,8b,15]

It was attempted to assign the electronic spectra (*i.e.*, different electronic transitions) based on molecular orbital and population analyses for the Λ-Cu-*R*-L^1 diastereomer.[5–8,24–26] For open shell transition-metal complexes (as in the present case), a large number of excitations occur at a single excited state (wavelength) (Table S1, ESI†), which make the assignment protocol complicated. However, some selected and simplified assignments on electronic spectra are listed in Table 3, which are comparable to the experimental data. Thus, the band at 681 nm comprises a combination from MM and ML/LM transitions with significant oscillator strength (f) of 0.0011, mostly due to HOMO−17 to LUMO excitation with the highest molecular orbital (MO) contribution of 63%. The HOMO−17 orbital is mainly localized on the metal d_{xy}-/ligand (sal-ring) π-moieties, while the LUMO is

Table 2 Selected bond lengths (Å) and angles (°) in *R*-HL^1 and in the diastereomeric pair Δ-Cu-*R*-L^1/Λ-Cu-*R*-L^1

	PXRD structures			
Bond length (Å) & angles (°)	*R*-HL^1 [b]	Δ-Cu-*R*-L^1	Λ-Cu-*R*-L^1	X-ray structure[a] Δ-Cu-*R*-L
Cu—O1/Cu—O2		1.873/1.870	1.887/1.913	1.870(2), /1.880(2)
Cu—N1/Cu—N2		1.993/1.984	1.995/1.991	2.021(3), /1.976(3)
O1—Cu—O2		151.7	149.6	151.56(12)
N1—Cu—N2		150.5	164.2	151.94(13)
N1—Cu—O1		92.7	88.2	86.13(12)
N2—Cu—O2		93.3	92.8	84.92(12)
N1—Cu—O2		93.4	89.5	101.63(12)
N2—Cu—O1		94.8	97.6	101.10(12)
O1—C1/C6—C7	1.392/1.503			
N1—C7/N1—C14	1.289/1.493			
C7—N1—C14	126.29			
C6—C7—N1	116.57			
C1—O1—H1	110.95			
θ/°		40.2	33.6	42.1
$\tau_{tet\text{-}sq}$ (θ/90°)		0.45	0.37	0.47

[a] From analogous bis[(*R*)-*N*-1-(phenyl)ethyl-salicylaldiminato]-Δ-copper(II), (Δ-Cu-*R*-L).[3a] [b] See values for X-ray structure in Table 1.

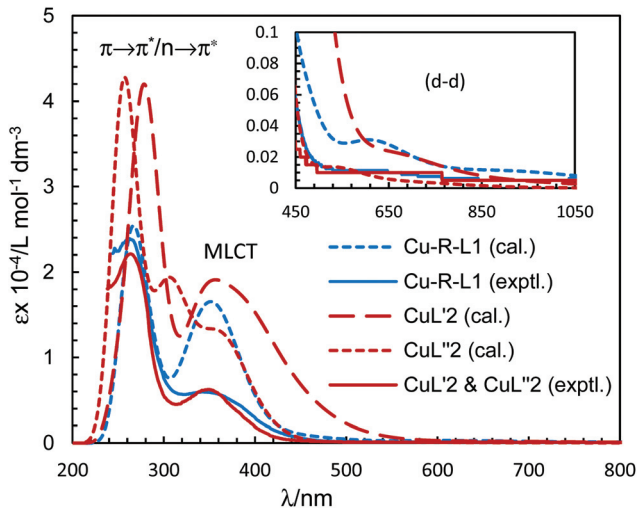

Fig. 7 Experimental UV-Vis spectrum for Cu-*R*-L^1 (identical to Cu-*S*-L^1) (0.04 mM) and CuL′$_2$/CuL″$_2$ (0.05 mM) in chloroform at 25 °C. Calculated spectra for Λ- or Δ-Cu-*R*-L^1, CuL′$_2$ and CuL″$_2$ at the m06/sdd//b3lyp/6-31 g(d) level with PCM in chloroform (Gaussian band shape with exponential half-width, σ = 0.33 eV).

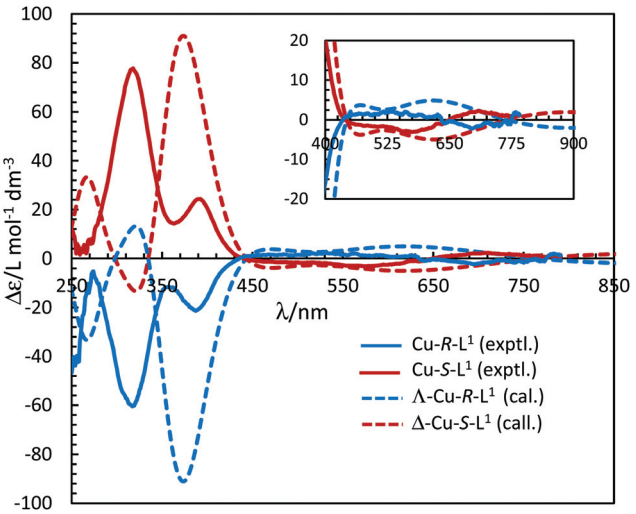

Fig. 8 Experimental ECD spectra for Cu-*R*-L^1/Cu-*S*-L^1 (1.21/1.33 mM) in chloroform at 25 °C (values of experimental $\Delta\varepsilon$ are increased by 5 times). Calculated spectra for Λ-Cu-*R*-L^1/Δ-Cu-*S*-L^1 at the m06/sdd//b3lyp/6-31 g(d) level with PCM in chloroform (Gaussian band shape with exponential half-width σ = 0.33 eV). See Fig. S5b, ESI† for the calculated spectra of the opposite Δ-Cu-*R*-L^1/Λ-Cu-*S*-L^1 configuration.

localized on the metal d_{z^2}-/ligand (sal-ring) π-moieties. This band is very close to the experimental d–d (MM) transition band at *ca.* 650 nm (Fig. 7, inset, Table 3). Similarly, the band at 607 nm consists of a combination from MM, ML/LM and LL transitions (f = 0.0053), and mainly assigns for metal d_{z^2}-/ligand σ-moieties (HOMO−22) to metal d_{z^2}-/ligand (sal-ring) π-moieties (LUMO) excitation with MO contributions of 40%. However, the HOMO to LUMO excitation, which occurs at 430 nm (f = 0.0085, MOs = 42%), comprises a combination from MM and ML/LM transitions. This later band is assigned mainly for metal $d_{x^2-y^2}$-/ligand (sal-ring) π-moieties (HOMO) to metal d_{z^2}-/ligand (sal-ring) π-moieties (LUMO) excitation. Indeed, there are some other intense bands on the computed spectra, very close to the experimental bands (Table 3). The frontier molecular orbitals (MOs) for HOMO, HOMO−17, HOMO−22 and LUMO are illustrated in Fig. 9.

Optimized structures and excited state properties (diastereoselection and chirality induction at-metal)

The four-coordinated non-planar metal(II)-complexes with chiral N,O-chelate Schiff base ligands exhibit Λ *vs.* Δ-chirality induction at-metal. The enantiopure *R*- or *S*-N,O ligands provide two opposite configured diastereomers of C_2-symmetry with Δ-Cu and Λ-Cu.[3–9,15] In order to determine the Λ *vs.* Δ-chirality, we optimized the structures for diastereomeric pairs Δ-Cu-*R*-L^1/Λ-

Table 3 Selected and simplified assignments on electronic spectra calculated for Λ-Cu-*R*-L^1 at the m06/sdd//b3lyp/631 g(d) level

Bands[a] (λ/nm)	Oscil. strength. (f)	Excitations[b] (MOs contribution, %)	Assignments[c,d]
681 (~650)	0.0011	H-17 → L (63), H-16 → L (35)	MM, ML/LM
607	0.0053	H-22 → L (40), H-2 → L (23)	MM, ML/LM, LL
430	0.0085	H → L (42), H → L + 2 (16)	MM, ML/LM
363 (342)	0.1245	H → L + 1 (14), H → L + 2 (26)	ML, LL
333	0.0765	H-5 → L (63), H-3 → L (14)	LM, LL
263 (259)	0.0852	H → L + 7 (20), H → L + 12 (13)	ML, LL

[a] Experimental values are in parentheses. [b] H/L = HOMO/LUMO. [c] MM = metal centered d–d, ML = metal–ligand and LL = intra-ligand transitions, respectively. [d] Assigned for β-spin MOs consideration.

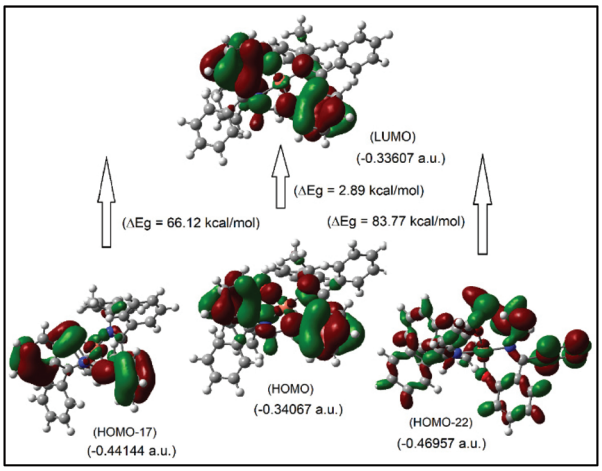

Fig. 9 The frontier MOs of HOMO, HOMO–17, HOMO–22 and LUMO for Λ-Cu-*R*-L^1 (calculated at m06/sdd//b3lyp/631 g(d)), for β-spin considerations.

Cu-*R*-L^1 and Δ-Cu-*S*-L^1/Λ-Cu-*S*-L^1 at the b3lyp/6-31 g(d) level (Fig. S1, ESI†). The results suggest that the Λ-Cu-*R*-L^1 and Δ-Cu-*S*-L^1 diastereomers are more stable than the corresponding Δ-Cu-*R*-L^1 and Λ-Cu-*S*-L^1 diastereomers by *ca.* 7.60 kcal mol^{-1}. The excited state properties by TDDFT, calculated for the diastereomeric pairs Δ-Cu-*R*-L^1/Λ-Cu-*R*-L^1 and Δ-Cu-*S*-L^1/Λ-Cu-*S*-L^1 at m06/sdd with PCM in chloroform, provide UV-Vis and ECD spectra, which can be compared to the experimental spectra in solution (Fig. 7 and 8). The experimental and calculated UV-Vis spectra for both diastereomeric pairs are, as expected, essentially identical (Fig. S3†), while the ECD spectra show mirror-image relationships (Fig. 8 and Fig. S3, ESI†). ECD spectra indicate diastereomeric excess and allow to determine the absolute configuration by comparison with spectra of known structures or with calculated spectra. Here we compare the experimental and computed ECD spectra to assign the absolute configuration of the metal-centre (*i.e.*, Λ-M *vs.* Δ-M).[3–8,15] The experimental spectra for Cu-*R*-L^1 or Cu-*S*-L^1 fit well to the computed spectra for the Λ-Cu-*R*-L^1 or Δ-Cu-*S*-L^1 diastereomer with slight shifting of the band positions (Fig. 8; the opposite comparison is given in Fig. S5b, ESI†). This and the optimized structures (in the gas phase) strongly indicate Λ-Cu-*R*-L^1 or Δ-Cu-*S*-L^1 as major diastereomers in solution for the *R*- or *S*-N,O ligated complexes, respectively. For the calculated ECD spectra for the opposite Δ-Cu-*R*-L^1/Λ-Cu-*S*-L^1 configuration we note that the region of the d–d transition above 450 nm is similarly well reproduced for the Δ-Cu or Λ-Cu configuration regardless of the ligand enantiomer (Fig. S5b, ESI†). In the region of the ligand or charge-transfer transitions below 450 nm it is evident that the sign of $\Delta\varepsilon$ reverses with the wrong metal chirality for the given ligand enantiomer (Fig. 8 and Fig. S5b, ESI†). These results are in parallel to analogous bis[{(*R* or *S*)-*N*-(Ar)ethyl-2-oxo-1-naphthaldiminato-κ^{2}N,O}]Cu(II) (Scheme 3b)[5] both at solid-state and in solution. In the contrary, the preferred formation of Δ-Cu-*R*-L or Λ-Cu-*S*-L was reported (both at solid-state and in solution) in the analogous bis[(*R* or *S*)-*N*-1-(Ar)ethyl-salicylaldiminato-

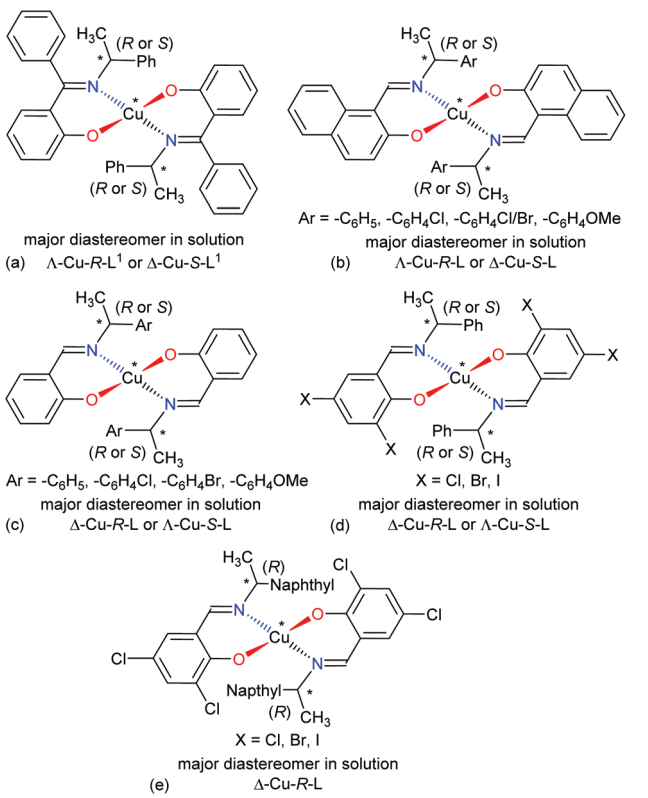

Scheme 3 Structural comparisons of Cu(II)-*chiral* Schiff bases complexes and their preferred diastereomer in solution: (a) this work, (b) ref. 5, (c) ref. 3*a*, (d) ref. 15, (e) ref. 2*g*.

κ²N,O]Cu(II) (Scheme 3c)[3a] and bis [*N*-(*R*)-1-(naphthyl)ethyl-3,5-dichlorosalicydenaminato]Cu(II) (Scheme 3e).[2g] Di-halogen substituents on the salicylal-ring favor Λ-Cu-*R*-L or Δ-Cu-*S*-L in bis[(*S* or *R*)-*N*-1-(phenyl)ethyl-(2,4-di-halogen-salicylaldiminato-κ²N,O)]Cu(II) (Scheme 3d)[15] at solid-state, which show helicity inversion to Δ-Cu-*R*-L or Λ-Cu-*S*-L in solution. The structural differences to the present complexes in Scheme 3a are (i) imino-hydrogen atom (Scheme 3b–e) instead of phenyl group, (ii) naphthyl ring (Scheme 3b) instead of salicylal ring, (iii) di-halogen substituents (Scheme 3d and 3e) on the salicylal ring, (iv) di-halogen substituents on the salicylal ring plus naphthyl group attached to the chiral carbon center (Scheme 3e). These results strongly suggest that an understanding and design of the ligand substituents can efficiently control the diastereoselection and *chirality* induction at-metal (*i.e.*, Δ *vs.* Λ).

Cyclic voltammetry (CV)

The cyclic voltammograms for Cu-*R*-L^1 were run at −1.00 to +0.80 V (*vs.* Ag/AgCl) at varying scan rates (*i.e.*, 0.10–0.30 V s^{-1}) in acetonitrile at 25 °C (Fig. 10). The reductive scans exhibit a strong broad cathodic peak centered at *ca.* −0.60 V at a scan rate of 0.10 V s^{-1}, which becomes more populated and is split into two strong peaks at *ca.* −0.43 V (*Ec*1) and −0.67 V (*Ec*2) with faster scan rates. These peaks are referred to two-electron charge-transfer processes for the $[Cu\text{-}R\text{-}L^1]^0/[Cu\text{-}R\text{-}L^1]^-$ (Cu^{2+}/Cu^+) and $[Cu\text{-}R\text{-}L^1]^-/[Cu\text{-}R\text{-}L^1]^{2-}$ (Cu^+/Cu^0) couples (L^1 = deprotonated Schiff base ligand), respectively. The oxidative scans reveal two corresponding weak anodic peaks at *ca.* −0.25 V (*Ea*2) and +0.55 V (*Ea*1) for the $[Cu\text{-}R\text{-}L^1]^{2-}/[Cu\text{-}R\text{-}L^1]^-$ and $[Cu\text{-}R\text{-}L^1]^-/[Cu\text{-}R\text{-}L^1]^0$ couples, respectively. The relatively weak anodic peaks on the oxidative waves reflect instability of the oxidized species, which undergo chemical transformation and/or decomposition reaction. Indeed, a CV pattern run at the extended range from −1.00 to +1.20 V with a scan rate of 0.10 V s^{-1} shows a sharp anodic peak at *ca.* 0.97 V (Ea_{TBAP}) for the electrolyte (Fig. S10, ESI†).[8b] The CV results thus unequivocally demonstrate two quasi-reversible one-electron charge-transfer processes for the Cu^{2+}/Cu^+ and Cu^+/Cu^0 couples in acetonitrile.[5,8b,24–27] Analyses of voltammograms at variable scan rates exhibit that the cathodic and anodic peaks become increasingly populated and shift to lower and higher potentials, respectively with faster scan rates (Fig. 10). Indeed, a plot of cathodic peak current *versus* square root of scan rates (*i.e.*, *Ic*2 *vs.* $\nu^{1/2}$) reflects a linear relationship (Fig. S11, ESI†), suggesting a diffusion-controlled electrochemical process in solution.[8b,24–26]

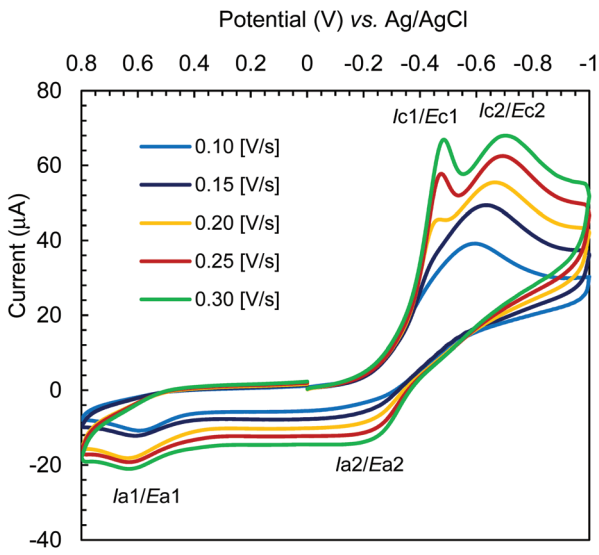

Fig. 10 Cyclic voltammograms for Cu-*R*-L^1 (0.5 mM); TBAP (0.1 M) at varying scan rates 0.10–0.30 [V s^{-1}] in acetonitrile at 25 °C.

Experimental

Materials and methods

IR spectra were recorded on a Nicolet iS10 spectrometer as KBr discs at ambient temperature. UV-Vis spectra were recorded with a Shimadzu UV 1800 spectrophotometer in methanol at 25 °C. ECD spectra were obtained with a JASCO Spectropolarimeter (J715) in chloroform at 20 °C. Elemental analyses were run on a Vario EL instrument from Elementaranalysensysteme. ^{1}H NMR spectra were measured on a Bruker Avance DPX 400 spectrometer at 20 °C with calibration against the residual protonated solvent signal of $CDCl_3$ (δ = 7.26 ppm). Electron impact (EI) mass spectra were recorded with a Thermo-Finnigan TSQ 700. Isotopic distribution patterns for the $^{63/65}$Cu containing ions were clearly visible in the spectra. An Epsilon™ instrument (BASi) electrochemical analyser was used for running cyclic voltammograms with tetra-*N*-butyl-ammonium hexafluorophosphate (TBAP) as supporting electrolyte in acetonitrile at 25 °C. A three-electrode measurement system was used, composed of a platinum disc working electrode, a platinum wire auxiliary electrode and an Ag/AgCl reference electrode, respectively. The solution containing the sample and TBAP was deoxygenated with purging nitrogen gas for about 10 minutes prior to use. The working electrode was cleaned with the supplied solution and dried prior to each scan to avoid any contamination due to deposition of the metal. Reproducibility of the CV patterns was checked at a scan rate of 0.10 V s^{-1} in acetonitrile.

General procedure to synthesize the Schiff base ligands (*R*- or *S*-HL)

Hydroxy-benzophenone (HL′, 12.07 mmol) was dissolved in 20 mL of methanol and 3–4 drops of concentrated H_2SO_4 were added into the solution which was then stirred for *ca.* 10 min. An equimolar amount of enantiopure (*R* or *S*)-(phenyl)ethylamine (dissolved in 5 mL of methanol) was added into this solution slowly. The reaction mixture was then refluxed for 5–6 h and the colour changed to yellow-orange. Thin-layer chromatography (TLC) was run to monitor the progress of the reaction. After completion of the reaction, the solvent was evaporated to *ca.* 50% *in vacuo* and this solution was left standing for crystallization. After 3–4 d, microcrystals were formed,

filtered off and washed two times with methanol (1 mL) followed by *n*-hexane (1 mL). The microcrystals were dried in air for 3–4 days and the obtained solid yellow-orange products were analyzed as 2-{(*E*)-((*S*)-1-(phenyl)ethylimino)(phenyl)methyl}phenol (*R*- or *S*-HL^1). The same procedure was followed for the synthesis of 2-{(*E*)-((*S*)-1-(*p*-methoxyphenyl)ethylimino)(phenyl)methyl}phenol (*R*- or *S*-HL^2) using (*R* or *S*)-(*p*-methoxyphenyl)ethylamine. Bright-yellow single crystals of *R*-HL^1 in X-ray quality were obtained *via* recrystallization or slow evaporation from concentrated methanol solution.

2-{(*E*)-((*S*)-1-(Phenyl)ethylimino)(phenyl)methyl}phenol (*S*-HL^1). Yield: 2.10 g (73%, based on HL′). – IR (KBr, cm^{-1}): ν = 3065, 3034, 2979, 2929w (C–H), 1604vs, 1598sh (C═N) and 1572vs (C═C). – ^{1}H NMR (400 MHz, $CDCl_3$): δ = 1.57 (d, J_{HH} = 6.8 Hz, 3H, CH_3), 4.55 (q, J_{HH} = 6.8 Hz, 1H, C*H*), 6.67 (t, J_{HH} = 7.4 Hz, 1H, H_{Ar}), 6.79 (dd, J_{HH} = 8.0, 1.6 Hz, 1H, H_{Ar}), 7.11 (d, J_{HH} = 8.0 Hz, 1H, H_{Ar}), 7.18 (m, 1H, H_{Ar}), 7.25–7.28 (m, 4H, H_{Ar}), 7.30–7.36 (m, 3H, H_{Ar}) and 7.53–7.56 (m, 3H, H_{Ar}).

2-{(*E*)-((*R*)-1-(Phenyl)ethylimino)(phenyl)methyl}phenol (*R*-HL^1). Yield: 2.04 g (71%, based on HL′). – IR (KBr, cm^{-1}): ν = 3061, 3030, 2974, 2922w (C–H), 1605vs, 1595sh (C═N) and 1570vs (C═C). – ^{1}H NMR (400 MHz, $CDCl_3$): δ = 1.56 (d, J_{HH} = 6.8 Hz, 3H, CH_3), 4.54 (q, J_{HH} = 6.8 Hz, 1H, C*H*), 6.67 (t, J_{HH} = 7.4 Hz, 1H, H_{Ar}), 6.79 (dd, J_{HH} = 8.0, 1.6 Hz, 1H, H_{Ar}), 7.08 (d, J_{HH} = 8.4 Hz, 1H, H_{Ar}), 7.18 (m, 1H, H_{Ar}), 7.26–7.28 (m, 4H, H_{Ar}), 7.29–7.36 (m, 3H, H_{Ar}) and 7.53–7.55 (m, 3H, H_{Ar}).

2-{(*E*)-((*S*)-1-(*p*-Methoxyphenyl)ethylimino)(phenyl)methyl}phenol (*S*-HL^2). Yield: 2.50 g (77%, based on HL′). – IR (KBr, cm^{-1}): ν = 3057, 3030, 2995, 2928w (C–H), 1604 (C═N) and 1570vs (C═C). – ^{1}H NMR (400 MHz, $CDCl_3$): δ = 1.54 (d, J_{HH} = 6.8 Hz, 3H, CH_3), 3.82 (s, 3H, OCH_3), 4.51 (q, J_{HH} = 6.6 Hz, 1H, C*H*), 6.66 (dt, J_{HH} = 8.0, 0.8 Hz, 1H, H_{Ar}), 6.80 (dd, J_{HH} = 8.0, 1.6 Hz, 1H, H_{Ar}), 6.88 (d, J_{HH} = 8.4 Hz, 2H, H_{Ar}), 7.04 (d, J_{HH} = 8.4 Hz, 2H, H_{Ar}), 7.20 (d, J_{HH} = 8.4 Hz, 2H, H_{Ar}), 7.30 (dt, J_{HH} = 8.4, 1.6 Hz, 2H, H_{Ar}) and 7.53–7.55 (m, 3H, H_{Ar}).

2-{(*E*)-((*R*)-1-(*p*-Methoxyphenyl)ethylimino)(phenyl)methyl}phenol (*R*-HL^2). Yield: 2.40 g (74%, based on HL′). – IR (KBr, cm^{-1}): ν = 3057, 3032, 2997, 2930w (C–H), 1605 (C═N) and 1568vs (C═C). – ^{1}H NMR (400 MHz, $CDCl_3$): δ = 1.53 (d, J_{HH} = 6.8 Hz, 3H, CH_3), 3.82 (s, 3H, OCH_3), 4.51 (q, J_{HH} = 6.6 Hz, 1H, C*H*), 6.66 (dt, J_{HH} = 8.0, 0.8 Hz, 1H, H_{Ar}), 6.79 (dd, J_{HH} = 8.0, 1.6 Hz, 1H, H_{Ar}), 6.88 (d, J_{HH} = 8.8 Hz, 2H, H_{Ar}), 7.02 (d, J_{HH} = 8.4 Hz, 1H, H_{Ar}), 7.04 (d, J_{HH} = 9.6 Hz, 1H, H_{Ar}), 7.19 (d, J_{HH} = 8.8 Hz, 2H, H_{Ar}), 7.27–7.32 (m, 2H, H_{Ar}) and 7.46–7.57 (m, 3H, H_{Ar}).

General procedure to synthesize the complexes (Cu-*S*- or -*R*-L)

The enantiopure Schiff base ligand, 2-{(*E*)-((*R* or *S*)-1-(phenyl)ethylimino)(phenyl)methyl}phenol (*R*- or *S*-HL^1) (239.3 mg, 1 mmol) was dissolved in 10 mL of methanol, which was then poured into 5 mL of a methanolic solution of Cu(II) acetate (99.8 mg, 0.5 mmol). The reaction mixture was refluxed for 6–7 hours and a green product precipitated, which was then cooled at room temperature. The green product was separated by filtration and washed with methanol three times (1 mL each). The product was dried in air for 2–3 days to give deep-green microcrystals of bis[(*R* or *S*)-2-((*E*)-1-(1-(phenyl)ethylimino)ethyl)phenolato-κ^{2}N,O]-Λ/Δ-copper(II) (Λ/Δ-Cu-*S*- or -*R*-L^1). The same procedure was followed to synthesize bis[(*R* or *S*)-2-((*E*)-1-(1-(*p*-methoxyphenyl)ethylimino)ethyl)phenolato-κ^{2}N,O]-Λ/Δ-copper(II) (Λ/Δ-Cu-*S*- or -*R*-L^2) using the enantiopure Schiff base ligands of *R*- or *S*-HL^2.

Bis[(*R* or *S*)-2-((*E*)-1-(1-(phenyl)ethylimino)ethyl)phenolato-κ^{2}N,O]-Λ/Δ-copper(II), (Λ/Δ-Cu-*R*- or *S*-L^1). Yield 225 mg (68%). – IR (KBr, cm^{-1}): ν = 3059, 3028, 2972, 2926w (C–H), 1607vs (C═N) and 1570 (C═C).

Bis[(*R* or *S*)-2-((*E*)-1-(1-(*p*-methoxyphenyl)ethylimino)ethyl)phenolato-κ^{2}N,O]-Λ/Δ-copper(II), (Λ/Δ-Cu-*R*- or *S*-L^2). Yield 256 mg (71%). – IR (KBr, cm^{-1}): ν = 3152, 2986, 2936w (C–H), 1616sh, 1605 (C═N) and 1570 vs (C═C).

Crystallization of Cu-*S*- or -*R*-L^1 to yield CuL′$_2$ and CuL″$_2$

Deep-green block-shaped single crystals in X-ray quality were obtained *via* slow diffusion of methanol into a concentrated solution of Cu-*S*- or -*R*-L^1 in dichloromethane after 3–4 days. Single-crystal X-ray results show the formation of bis[2-oxo-benzophenonato-κ^{2}O,O′]-copper(II), (CuL′$_2$) as product from the crystallization experiment with about equal admixture of bis[2-(imino(phenyl)methyl)phenolato-κ^{2}N,O]copper(II), (CuL″$_2$) (Scheme 2) *via in situ* hydrolysis of the coordinated Schiff bases back to 2-hydroxy-benzophenone (HL′) and to 2-(imino(phenyl)methyl)phenol (HL″), which in-turn bind with the copper(II) ion to form the mixture of complexes during crystallization. However, several attempts were made to grow suitable single crystals of Cu-*S*- or *R*-L^1 in X-ray quality, but failed due to the *in situ* hydrolysis of the ligands in the complexes.

Mixed product of bis[2-oxo-benzophenonato-κ^{2}O,O′]-copper (II), (CuL′$_2$) and bis[2-(imino(phenyl)methyl)phenolate-κ^{2}N,O] copper(II), (CuL″$_2$): – IR (KBr, cm^{-1}): ν = 3325 (N–H), 3056, 3013, 2974w (C–H), 1601/1579vs (C═N/O) and 1559s (C═C). – IR (calculated for CuL′$_2$, cm^{-1}): ν = 3227, 3208, 3182 (C–H), 1670, 1639 (C═C), 1605 (C═O) and 1571 (C═C). – IR (calculated for CuL″$_2$, cm^{-1}): ν = 3519, 3517 (N–H), 3222, 3210, 3178 (C–H), 1667, 1640 (C═C), 1621 (C═N) and 1574 (C═C). – EI-MS (at 100 °C): 301 (55) [*S*- or *R*-HL^1]$^+$, 197 (25) [HL″]$^+$, 196 (100) [HL″-H]$^+$ and 105 (60) [{C_6H_5CHO}-H]$^+$. EI-MS (at 240 °C): 457 (11) [CuL′$_2$ = Cu{(C_6H_4O)(C_6H_5)CO}$_2$]$^+$, 456 (10) [CuL′L″ = Cu{(C_6H_4O)(C_6H_5)CO}{(C_6H_4O)(C_6H_5)CNH}]$^+$, 455 (7) [CuL″$_2$ = Cu{(C_6H_4O)(C_6H_5)CNH}$_2$]$^+$, 260 (43) [CuL′]$^+$, 258 (33) [CuL″-H]$^+$, 198 (60) [HL′]$^+$, 197 (100) [HL″]$^+$, 121 (61) [{(C_6H_4OH)CHO}-H]$^+$ and 105 (37) [{C_6H_5CHO}-H]$^+$. Elemental analysis: calc. for CuL′$_2$ ($C_{26}H_{18}CuO_4$, M = 457.96 g mol^{-1}) C 68.19, H 3.96; calc. for CuL″$_2$ ($C_{26}H_{20}CuN_2O_2$, M = 456.01 g mol^{-1}) C 68.49, H 4.42, N 6.14: found C 68.44, H 4.48, N 2.63%.

X-ray crystallography

Suitable single-crystals of *R*-HL^1 and from the crystallization product of Cu-*R*-L^1, that is the mixture of CuL′$_2$ and CuL″$_2$ were carefully selected under a polarizing microscope and mounted on a loop. *Data collection*: Kappa APEX2 Duo CCD diffractometer with a microfocus source and multi-layer mirror

Table 4 X-ray crystal data and structure refinement parameters for *R*-HL[1] and CuL′$_2$/CuL″$_2$

Identification code	*R*-HL[1]	CuL′$_2$/CuL″$_2$
Empirical formula	$C_{21}H_{19}NO$	$C_{26}H_{18.88}CuN_{0.88}O_{3.12}$
M (g mol^{-1})	301.37	457.08
Crystal size (mm^3)	0.25 × 0.25 × 0.10	0.16 × 0.09 × 0.04
Temperature (K)	140	140
θ range (°) (completeness)	4.4–67.6° (0.99)	2.5–27.6° (0.999)
h, k, l range	$h = -11 \rightarrow 11$	$h = -24 \rightarrow 22$
	$k = -9 \rightarrow 9$	$k = -7 \rightarrow 7$
	$l = -13 \rightarrow 13$	$l = -25 \rightarrow 25$
Crystal system	Monoclinic	Monoclinic
Space group	$P2_1$	$C2/c$
a (Å)	9.9056(5) Å	18.4742(15) Å
b (Å)	8.1390(4) Å	5.8299(5) Å
c (Å)	10.8874(5) Å	19.8803(17) Å
β (°)	111.182 (2)°	113.803 (4)°
V (Å^3)	818.46(7) Å^3	1959.0(3) Å^3
Z	2	4
D_{calc} (g cm^{-3})	1.223	1.550
Radiation source (Å)	Cu Kα, λ = 1.54178	Mo Kα, λ = 0.71073
μ (mm^{-1})	0.58	1.15
F (000)	320	940
Max./min. transmission	1.000/0.893	1.000/0.908
Reflect. Collected	22 837	10 309
Independent reflections (R_{int})	2955 (0.034)	2278
Data/restraints/parameters	2955/1/212	2278/1/150
Max./min. $\Delta\rho^a$ (e Å^{-3})	0.10/−0.14	0.46/−0.31
R_1/wR_2 [$I > 2\sigma(I)$]^b	0.0258/0.0658	0.0376/0.1039
R_1/wR_2 (all data)^b	0.0261/0.0658	0.0463/0.1093
Goodness-of-fit (GOF) on $F^{2\,c}$	1.04	1.05
Flack parameter^d	0.04 (7)	—

^{a} Largest difference peak and hole. ^{b} $R_1 = [\sum(||F_o| - |F_c||)/\sum |F_o|]$; w$R_2 = [\sum [w(F_o^2 - F_c^2)^2]/\sum [w(F_o^2)^2]]^{1/2}$. ^{c} Goodness-of-fit = $[\sum [w(F_o^2 - F_c^2)^2]/(n-p)]^{1/2}$. ^{d} Absolute structure parameter.[34]

monochromator for Cu–Kα radiation (λ = 1.54178 Å) for *R*-HL[1] and Mo-Kα radiation (λ = 0.71073 Å) for CuL′$_2$/CuL″$_2$ at 140(2) K; ω-scans (Table 4). Data collection and cell refinement with APEX2,[28] data reduction with SAINT (Bruker).[29] *Structure analysis and refinement*: The structures were solved by intrinsic phasing (SHELXT-2015),[30] refinement was done by full-matrix least squares on F^2 using the SHELXL-2017 program suite,[30] empirical (multi-scan) absorption correction with SADABS (Bruker).[31] All non-hydrogen atom positions in *R*-HL[1] were refined with anisotropic temperature factors. In the metal complex the Cu atom sits on an inversion center, rendering the two ligands symmetry equivalent. When the metal complex was refined as bis[2-oxo-benzophenonato-κ^{2}O,O′]-copper(II), (CuL′$_2$) a large residual electron density of 0.52 e Å^{-3} was found in a hydrogen-bond distance to the keto oxygen atom. The IR spectrum showed a sharp band at 3325 cm^{-1} for ν(N–H) (Fig. S6c, ESI†) and the CHN elemental analysis gave a nitrogen content of 2.63 wt%. Subsequently, the keto O atom has been refined as a split position of O and NH using PART commands, with about equal occupancy (the occupancy was free to refine). This split position of NH then corresponded to the complex bis[2-(imino(phenyl)methyl)phenolato-κ^{2}N,O] copper(II), (CuL″$_2$). This split N atom could only be refined isotropically, while the rest of the atoms have been refined anisotropically. The hydrogen atom of the NH group was found and refined with U_{iso}(H) = 1.5U_{eq}(N). The NH distance had to be restrained with DFIX.

Hydrogen atoms for aromatic CH, aliphatic CH and CH_3 groups were positioned geometrically (C–H = 0.95 Å for aromatic CH, 1.00 Å for aliphatic CH and 0.98 Å for CH_3,) and refined using a riding model (AFIX 43 for aromatic CH, AFIX 13 for aliphatic CH, AFIX 137 for CH_3), with U_{iso}(H) = 1.2U_{eq}(CH) and U_{iso}(H) = 1.5U_{eq}(CH_3). The protic hydrogen for the OH group in *R*-HL[1] was positioned and refined freely with U_{iso}(H) = 1.5U_{eq}(O). Details of the X-ray structure determinations and refinements are provided in Table 4. Graphics were drawn with DIAMOND (Version 4.6.4).[32] Computations on the supramolecular interactions were carried out with PLATON for Windows.[33] The structural data for this paper has been deposited with the Cambridge Crystallographic Data Center (CCDC-numbers 2060528 for *R*-HL[1], 2060529 for CuL′$_2$/CuL″$_2$†).

Powder X-ray diffraction (PXRD)

Powder X-ray diffraction (PXRD) data for *R*-HL[1] and Cu-*R*-L[1] were collected on a GNR Explorer powder X-ray diffractometer, operating in Bragg–Brentano geometry with Cu target at 30 kV and 20 mA. A zero background sample holder was used to filter signals from the sample holder, while a Ni (nickel) filter was used to cut the beta (K_β) radiation. Data collections were carried out at 298 K with a step size 0.02° and an integration time of 3 s per step over an angular range of 5–50° (2θ). All steps to determine the crystal structure for Cu-*R*-L[1] were performed using the program Expo-2014.[20a] The background of the diffraction pattern was modelled by a shifted Chebyshev

function (number of coefficients 15). The selected 20 peaks within 5–50° were indexed using the N-Treor09 module.[20b] The results suggested the possibility of three crystal systems with triclinic symmetry, among them the best one was chosen considering the figure of merit (M20), unit cell volume and peak positions. Density consideration indicated only one molecule of Cu-*R*-L^1 in the unit cell. Analysis of the powder pattern by the FINDSPACE module of Expo-2014 [20a] suggested the space group either as $P\bar{1}$ with a *non-chiral* or *P*1 with a *chiral* molecule in the asymmetric unit. Hence, the structure solution calculations were performed with the space group *P*1. We used DFT optimized structures for both diastereomers of Λ-Cu-*R*-L^1 and Δ-Cu-*R*-L^1 as input files for structure solution calculations, respectively. The solution was carried out by global optimization models using simulated annealing technique.[19b,21] A total of 14 structural variables were used for structure solution. The Cu atom was selected as the center of rotation and anti-bump restraints were applied to C, N and O atoms. Among 10 trial structures, the best one was chosen based on crystal packing and minimum difference between calculated and experimental patterns, which was used as the initial structural model for Rietveld refinement.[22,23] In Rietveld refinement, standard restraints were applied only to the phenyl rings.[21,22d,23b,c] Hydrogen atoms bonded to the carbon atoms were placed automatically at calculated positions. The summary of crystal data and structure refinement parameters are listed in Table 5.

Computational method

A thorough computational procedure was performed with Gaussian 09[35] to rationalize the experimental results and thereby to gain insight into diastereoselection and Λ *vs.* Δ-*chirality* induction at-metal. The metal(II)-*chiral* N,O-chelate Schiff base complexes in tetrahedral or distorted-tetrahedral geometry demonstrate *chirality* induction at the metal centre (Λ-Cu and Δ-Cu), and hence, provide two diastereomers of opposite configuration along with C_2-symmetry of the molecule.[3–8,15] Thus, we optimized the diastereomeric pairs Λ-Cu-*R*-L^1/Δ-Cu-*R*-L^1 and Λ-Cu-*S*-L^1/Δ-Cu-*S*-L^1 at the b3lyp/6-31 g(d) level (Fig. S1, ESI†). The gas-phase initial geometries for these diastereomeric pairs were generated from X-ray structures of the analogous bis[(*R* or *S*)-*N*-1-(phenyl)ethyl-salicylaldiminato-κ^{2}N,O]-Λ or Δ-Cu(II)[3a] by replacing the imino-hydrogen atom with the phenyl group. It was attempted to optimize the hydrolysed products from crystallization of Cu-*R*-L^1 such as bis[2-oxo-benzophenonato-κ^{2}O,O′]-copper(II), (CuL′$_2$) and bis[2-(imino(phenyl)methyl)phenolato-κ^{2}N,O]copper(II) (CuL″$_2$) at the b3lyp/6-31 g(d) level (Fig. S2, ESI†), respectively. The gas-phase initial geometries for these complexes were generated from their X-ray structures. The excited state properties (*e.g.*, UV-Vis and ECD spectra) for the diastereomeric pairs (Λ-Cu-*R*-L^1/Δ-Cu-*R*-L^1 and Λ-Cu-*S*-L^1/Δ-Cu-*S*-L^1) and for CuL′$_2$/CuL″$_2$ were calculated by TDDFT at the m06/sdd level (Fig. 7, 8 and Fig. S3, ESI†).[5,15] The polarization continuum model (PCM) using chloroform as solvent was employed and 72 excited states (roots) were considered for calculations (Table S1, ESI†). Indeed, excited state properties were calculated at different combinations of the functionals and the basis sets such as b3lyp/sdd, b3lyp/svp and m06/tzvp, respectively, for Λ-Cu-*R*-L^1 (Fig. S4 and S5a, ESI†). The results are almost identical spectra with little shifting of band maxima, which strongly support the reliability and validity of the methods used. However, the best fit to experimental spectra was found at the m06/sdd// b3lyp/6-31 g(d) level (Fig. 7 and 8). In addition, assignments on electronic spectra were performed at the same level of theory for Λ-Cu-*R*-L^1 (Table 5). The spectra were generated using the program SpecDis[36] by applying Gaussian band shape with exponential half-width σ = 0.33 eV.

Table 5 PXRD data and structure refinement parameters for *R*-HL^1, Λ-Cu-*R*-L^1 and Δ-Cu-*R*-L^1

Compound	*R*-HL^1	Λ-Cu-*R*-L^1	Δ-Cu-*R*-L^1
Empirical formula	$C_{21}H_{19}NO$	$C_{42}H_{36}CuN_2O_2$	
M (g mol^{-1})	301.4	664.3	
Temperature T (K)	298		
Crystal system	Monoclinic	Triclinic	
Radiation source (Å)	Cu Kα, 1.54056		
Space group	$P2_1$	*P*1	
a (Å)	10.964	10.126	10.119
b (Å)	8.306	9.382	9.374
c (Å)	9.997	9.346	9.342
α (°)	90.00	91.58	91.39
β (°)	111.45	114.45	114.42
γ (°)	90.00	83.31	83.30
Volume (Å^3)	847.28	802.48	801.07
D_{calc} (g cm^{-3})	1.177	1.377	
Z	2	1	
2θ range (°)	5.00–50.00		
Step size (2θ/°)	0.02		
Counting time (s)	3		
No. of counts	4502		
No. of reflections	171	274	
No. of background points	20		
R_p	4.568	6.521	6.881
R_{wp}/R_{exp}	6.354/2.363	10.637/2.312	10.992/2.315
χ^2	7.23	21.177	22.547
Goodness-of-fit	2.689	4.601	4.748

Conclusions

The pseudotetrahedral complex bis[(*R* or *S*)-2-((*E*)-1-(1-(Ar)ethylimino)ethyl)phenolato-κ^{2}N,O]-Λ/Δ-copper(II), (Λ/Δ-Cu-*S*- or *R*-L) was investigated as a potential candidate to exhibit induced chirality at-metal, that is formation of the Δ-Cu-*S* or Λ-Cu-*R* diastereomer for *S*- or *R*-HL ligands. Formation of the intact complexes is confirmed by decomplexation reaction with NaCN, which provides the free Schiff base ligands in DMSO-d$_6$ solution. PXRD structure determinations for Cu-*R*-L^1 showed two phenolate-oxygen and two imine-nitrogen atoms from two Schiff base ligands to coordinate to copper(II) in a pseudotetrahedral geometry with Λ/Δ-chirality induction at-metal. Yet, PXRD structure determination did not allow to determine the absolute configuration unlike single-crystal X-ray diffractometry. Optimized gas-phase structures by DFT indicate the Δ-Cu-*S*-L or Λ-Cu-*R*-L diastereomer as slightly more stable. In the absence of single crystals for any of the Cu-*S*-L or Cu-*R*-L complexes and also to assess the diastereo-

selectivity in solution, we had to resort to electronic circular dichroism (ECD) in combination with theoretical calculations. Experimental solution ECD spectra show an expected mirror-image relationship and upon comparison with calculated ECD spectra suggest the preferred formation of the Δ-Cu-*S*-L or Λ-Cu-*R*-L diastereomer (*i.e.*, diastereomeric excess) in solution. The present study adds a case to the understanding and design of the ligand substituents for controlling the diastereoselection and chirality induction at-metal (*i.e.*, Δ *vs.* Λ) in pseudotetrahedral Cu-Schiff-base complexes. Crystallization of Cu-*S*-L^1 or Cu-*R*-L^1 in MeOH/DCM failed due to *in situ* hydrolysis of the coordinated Schiff base ligands, as evidenced by X-ray structures determinations which yielded only Cu complexes of the hydrolysis products as bis[2-oxo-benzophenonato-κ^2O,O′]-copper(II) and bis[2-(imino(phenyl)methyl)phenolato-κ^2N,O] copper(II).

Conflicts of interest

There are no conflicts to declare.

Acknowledgements

We acknowledge the financial support from the Alexander von Humboldt Foundation (AvH), Bonn, Germany under the project "Research Group Linkage Program". We recognize the "Wazed Miah Science Research Centre" at Jahangirnagar University, Dhaka, Bangladesh for obtaining CV and PXRD data. Our sincere thanks to Professor Walid Houry and Vaibhav Bhandari, Department of Biochemistry, Faculty of Medicine, University of Toronto, for running ECD spectra. We thank Professor A. B. P. Lever, Department of Chemistry, York University, Toronto and the computecanada.ca (https://ccdb.computecanada.ca/) Ontario, for using computational resources.

Notes and references

1 (*a*) A. von Zelewsky, *Stereochemistry of Coordination Compounds*, John Wiley & Sons, Chichester, 1996, p. 69; (*b*) H. Amouri and M. Gruselle, *Chirality in Transition Metal Chemistry: Molecules, supramolecular assemblies and materials*, John Wiley & Sons, Chichester, 2008, p. 40; (*c*) E. C. Constable, *Chem. Soc. Rev.*, 2013, **42**, 1637; (*d*) H. Song, M. Postings, P. Scott and N. J. Rogers, *Chem. Sci.*, 2021, **12**, 1620; (*e*) K. A. Jensen, *Inorg. Chem.*, 1970, **9**, 1; (*f*) U. Knof and A. von Zelewsky, *Angew. Chem., Int. Ed.*, 1999, **38**, 302; (*g*) H. Brunner, M. Niemetz and M. Zabel, *Z. Naturforsch.*, 2000, **55b**, 145; (*h*) C. Evans and D. Luneau, *J. Chem. Soc., Dalton Trans.*, 2002, 83; (*i*) G. Brewer, C. Brewer, R. J. Butcher, G. T. Robichaux and C. Viragh, *Inorg. Chim. Acta*, 2014, **410**, 171; (*j*) R. E. Ernst, M. J. O'Connor and R. H. Holm, *J. Am. Chem. Soc.*, 1967, **89**, 6104; (*k*) E. C. Constable, G. Zhang, C. E. Housecroft, M. Neuburger and J. A. Zampese, *Chem. Commun.*, 2010, **46**, 3077; (*l*) F. Wang, H. Zhang, L. Li, H.-Q. Hao, X.-Y. Wang and J.-G. Chen, *Tetrahedron: Asymmetry*, 2006, **17**, 2059.

2 (*a*) H. Sakiyama, H. Okawa, N. Matsumoto and S. Kida, *Bull. Chem. Soc. Jpn.*, 1991, **64**, 2644; (*b*) H. Sakiyama, H. Okawa, N. Matsumoto and S. Kida, *J. Chem. Soc., Dalton Trans.*, 1990, 2935; (*c*) Z. Dezhahang, M. R. Poopari, J. Cheramy and Y. J. Xu, *Inorg. Chem.*, 2015, **54**, 4539; (*d*) H. Ōkawa, M. Nakamura and S. Kida, *Inorg. Chim. Acta*, 1986, **120**, 185; (*e*) T. Akitsu and Y. Einaga, *Polyhedron*, 2005, **24**, 2933; (*f*) T. Akitsu and Y. Einaga, *Polyhedron*, 2005, **24**, 1869; (*g*) T. Akitsu, *Polyhedron*, 2007, **26**, 2527; (*h*) T. Ohno, S. Chorazy, K. Imoto and S. Ohkoshi, *Cryst. Growth Des.*, 2016, **16**, 4119.

3 (*a*) A.-C. Chamayou, G. Makhloufi, L. A. Nafie, C. Janiak and S. Lüdeke, *Inorg. Chem.*, 2015, **54**, 2193; (*b*) A.-C. Chamayou, S. Lüdeke, V. Brecht, T. B. Freedman, L. A. Nafie and C. Janiak, *Inorg. Chem.*, 2011, **50**, 11363.

4 M. Enamullah, G. Makhloufi, R. Ahmed, B. Alif Joy, M. A. Islam, D. Padula, H. Hunter, G. Pescitelli and C. Janiak, *Inorg. Chem.*, 2016, **55**, 6449.

5 M. Enamullah, A. K. M. Royhan Uddin, G. Pescitelli, R. Berardozzi, G. Makhloufi, V. Vasylyeva, A.-C. Chamayou and C. Janiak, *Dalton Trans.*, 2014, **43**, 3313.

6 M. Enamullah, M. A. Quddus, M. R. Hasan, G. Pescitelli, R. Berardozzi, G. Makhloufi, V. Vasylyeva and C. Janiak, *Dalton Trans.*, 2016, **45**, 667.

7 (*a*) G. Pescitelli, S. Lüdeke, A.-C. Chamayou, M. Marolt, V. Justus, M. Górecki, L. Arrico, L. Di Bari, M. A. Islam, I. Gruber, M. Enamullah and C. Janiak, *Inorg. Chem.*, 2018, **57**, 13397; (*b*) M. Enamullah, M. A. Islam, B. A. Joy, B. Dittrich, G. J. Reiß and C. Janiak, *Inorg. Chim. Acta*, 2018, **482**, 935.

8 (*a*) M. Enamullah, V. Vasylyeva and C. Janiak, *Inorg. Chim. Acta*, 2013, **408**, 109; (*b*) M. Enamullah, M. A. Quddus, M. R. Hasan, G. Pescitelli, R. Berardozzi, G. J. Reiß and C. Janiak, *Eur. J. Inorg. Chem.*, 2015, 2758.

9 (*a*) S. E. Howson and P. Scott, *Dalton Trans.*, 2011, **40**, 4332; (*b*) J. M. Becker, J. Barker, G. J. Clarkson, R. van Gorkum, G. K. Johal, R. I. Walton and P. Scott, *Dalton Trans.*, 2010, **39**, 2309; (*c*) K. S. Min, A. H. Park, J. W. Shin, S. R. Rowthu, S. K. Kim and J. J. Ryoo, *Dalton Trans.*, 2010, **39**, 8741.

10 (*a*) O. Mamula, A. von Zelewsky, T. Bark, H. Stoeckli-Evans, A. Neels and G. Bernardinelli, *Chem. Eur. J.*, 2000, **6**(19), 3575; (*b*) R. Dreos, G. Nardin, L. Randaccio, P. Siega and G. Tauzher, *Inorg. Chem.*, 2004, **43**, 3433; (*c*) H. Dong, H. Hu, Y. Liu, J. Zhong, G. Zhang, F. Zhao, X. Sun, Y. Li and Z. Kang, *Inorg. Chem.*, 2014, **53**, 3434; (*d*) W. Huang and T. Ogawa, *Polyhedron*, 2006, **25**, 1379; (*e*) T.-Y. Li, Y.-X. Zheng and Y.-H. Zhou, *Dalton Trans.*, 2016, **45**, 19234.

11 (*a*) I. Katsuki, Y. Motoda, Y. Sunatsuki, N. Matsumoto, T. Nakashima and M. Kojima, *J. Am. Chem. Soc.*, 2002, **124**, 629; (*b*) S. Nagasato, I. Katsuki, Y. Motoda, Y. Sunatsuki, N. Matsumoto and M. Kojima, *Inorg. Chem.*, 2001, **40**, 2534; (*c*) D.-H. Ren, X.-L. Sun, L. Gu, D. Qiu, Z. Li and Z.-G. Gu, *Inorg. Chem. Commun.*, 2015, **51**, 50.

12 (*a*) T. Akitsu and Y. Einaga, *Acta Crystallogr., Sect. C: Cryst. Struct. Commun.*, 2004, **60**, m640; (*b*) C. T. Brewer,

G. Brewer, R. J. Butcher, E. E. Carpenter, A. Schmiedekamp and C. Viragh, *Dalton Trans.*, 2007, 295; (*c*) C. T. Brewer, G. Brewer, R. J. Butcher, E. E. Carpenter, A. M. Schmidekamp, C. Schmiedekamp, A. Straka, C. Viragh, Y. Yuzefpolskiy and P. Zavalij, *Dalton Trans.*, 2011, **40**, 181; (*d*) B. R. Groves, D. I. Arbuckle, E. Essoun, T. L. Lundrigan, R. Wang and M. A. S. Aquino, *Inorg. Chem.*, 2013, **52**, 11563; (*e*) R. Vadavi, E. D. Conrad, D. I. Arbuckle, T. S. Cameron, E. Essoun and M. A. S. Aquino, *Inorg. Chem.*, 2011, **50**, 11862.

13 (*a*) C. Merten, R. McDonald and Y. Xu, *Inorg. Chem.*, 2014, **53**, 3177; (*b*) M. Albrecht, E. Isaak, M. Baumert, V. Gossen, G. Raabe and R. Fröhlich, *Angew. Chem., Int. Ed.*, 2011, **50**, 2850; (*c*) C. M. álvarez, R. Carrillo, R. García-Rodríguez and D. Miguel, *Chem. Commun.*, 2011, **47**, 12765.

14 (*a*) J. Gregoliński, M. Hikita, T. Sakamoto, H. Sugimoto, H. Tsukube and H. Miyake, *Inorg. Chem.*, 2016, **55**, 633; (*b*) S. Zahn and J. W. Canary, *Science*, 2000, **288**, 1404.

15 N. Kordestani, H. A. Rudbari, G. Bruno, S. Rosario, J. D. Braun, D. E. Herbert, O. Blacque, I. Correia, M. Al-M. Zaman, M. Mamun Bindu, C. Janiak and M. Enamullah, *Dalton Trans.*, 2020, **49**, 8247.

16 (*a*) M. Enamullah, A. K. M. Royhan Uddin, A.-C. Chamayou and C. Janiak, *Z. Naturforsch., B: Chem. Sci.*, 2007, **62**, 807; (*b*) M. Enamullah, A. K. M. Royhan Uddin, G. Hogarth and C. Janiak, *Inorg. Chim. Acta*, 2012, **387**, 173.

17 (*a*) B. M. Drašković, G. A. Bogdanović, M. A. Neelakantan, A.-C. Chamayou, S. Thalamuthu, Y. S. Avadhut, J. Schmedt auf der Günne, S. Banerjee and C. Janiak, *Cryst. Growth Des.*, 2010, **10**, 1665; (*b*) K. Sarmah, G. Pandit, A. B. Das, B. Sarma and S. Pratihar, *Cryst. Growth Des.*, 2017, **17**, 368.

18 (*a*) A. J. McKinnon, T. N. Waters and D. Hall, *J. Chem. Soc.*, 1964, 3290; (*b*) D. Hall, A. J. McKinnon and T. N. Waters, *J. Chem. Soc.*, 1965, 425; (*c*) J. A. Bevan, D. P. Graddon and J. F. McConnell, *Nature*, 1963, **199**, 373; (*d*) G. Q. Zhang, G. Q. Yang and J. S. Ma, *J. Chem. Res.*, 2006, 19.

19 (*a*) M. Enamullah, A.-C. Chamayou, K. S. Banu, A.-C. Kautz and C. Janiak, *Inorg. Chim. Acta*, 2017, **464**, 186; (*b*) M. Enamullah, B. Alif Joy and M. K. Islam, *J. Mol. Struct.*, 2019, **1175**, 56.

20 (*a*) A. Altomare, C. Cuocci, C. Giacovazzo, A. Moliterni, R. Rizzi, N. Corriero and A. Falcicchio, *J. Appl. Crystallogr.*, 2013, **46**, 1231; (*b*) A. Altomare, C. Giacovazzo, A. Guagliardi, A. G. G. Moliterni, R. Rizzi and P.-E. Werner, *J. Appl. Crystallogr.*, 2000, **33**, 1180.

21 L. T. Wille, *Chem. Phys. Lett.*, 1987, **133**, 405.

22 (*a*) H. M. Rietveld, *Acta Crystallogr.*, 1967, **22**, 151; (*b*) B. M. Kariuki, D. M. S. Zin, M. Tremayne and K. D. M. Harris, *Chem. Mater.*, 1996, **8**, 565; (*c*) K. Užarević, V. Štrukil, C. Mottillo, P. A. Julien, A. Puškarić, T. Friščić and I. Halasz, *Cryst. Growth Des.*, 2016, **16**, 2342; (*d*) S. Mondal, M. Mukherjee, K. Dhara, S. Ghosh, J. Ratha, P. Banerjee and A. K. Mukherjee, *Cryst. Growth Des.*, 2007, **7**, 1716.

23 (*a*) R. Rahmani, A. Djafri, A. Chouaih, A. Djafri, F. Hamzaoui, R. Rizzi and A. Altomare, *J. Mol. Struct.*, 2017, **1143**, 259; (*b*) A. E. Watts, K. Maruyoshi, C. E. Hughes, S. P. Brown and K. D. M. Harris, *Cryst. Growth Des.*, 2016, **16**, 1798; (*c*) T. Dey, P. Chatterjee, A. Bhattacharya, S. Pal and A. K. Mukherjee, *Cryst. Growth Des.*, 2016, **16**, 1442.

24 M. Enamullah, M. Al-M. Zaman, M. M. Bindu, M. K. Islam and M. A. Islam, *J. Mol. Struct.*, 2020, **1201**, 127207.

25 M. Enamullah, M. A. Islam, B. A. Joy and G. J. Reiss, *Inorg. Chim. Acta*, 2016, **453**, 202.

26 M. Enamullah, M. A. Islam, A.-C. Kautz and C. Janiak, *J. Coord. Chem.*, 2018, **71**, 2557.

27 A. Zianna, G. Psomas, A. Hatzidimitriou and M. Lalia-Kantouri, *RSC Adv.*, 2015, **5**, 37495.

28 APEX2, *Data Collection Program for the CCD Area-Detector system, Version 2.1-0*, Bruker Analytical X-ray Systems, Madison, Wisconsin, USA, 2006.

29 *SAINT, data reduction and frame integration program for the CCD area-detector system*, Bruker Analytical X-ray Systems, Madison (WI), 2006.

30 G. Sheldrick, *Acta Crystallogr., Sect. A: Found. Crystallogr.*, 2008, **64**, 112.

31 G. M. Sheldrick, *Program SADABS*, University of Göttingen: Göttingen, Germany, 1996.

32 K. Brandenburg, *Diamond (Version 4), Crystal and Molecular Structure Visualization, Crystal Impact*, K. Brandenburg & H. Putz Gbr, Bonn, Germany, 2009–2020.

33 (*a*) A. L. Spek, *Acta Crystallogr., Sect. D: Biol. Crystallogr.*, 2009, **65**, 148; (*b*) A. L. Spek, *PLATON – A multipurpose crystallographic tool*, Utrecht University, Utrecht, The Netherlands, 2005.

34 (*a*) H. D. Flack, M. Sadki, A. L. Thompson and D. J. Watkin, *Acta Crystallogr., Sect. A: Found. Crystallogr.*, 2011, **67**, 21; (*b*) H. D. Flack and G. Bernardinelli, *Chirality*, 2008, **20**, 681; (*c*) H. D. Flack and G. Bernardinelli, *Acta Crystallogr., Sect. A: Found. Crystallogr.*, 1999, **55**, 908; (*d*) H. D. Flack, *Acta Crystallogr., Sect. A: Found. Crystallogr.*, 1983, **39**, 876.

35 M. J. Frisch, G. W. Trucks, H. B. Schlegel, G. E. Scuseria, M. A. Robb, J. R. Cheeseman, G. Scalmani, V. Barone, B. Mennucci, G. A. Petersson, H. Nakatsuji, M. Caricato, X. Li, H. P. Hratchian, A. F. Izmaylov, J. Bloino, G. Zheng, J. L. Sonnenberg, M. Hada, M. Ehara, K. Toyota, R. Fukuda, J. Hasegawa, M. Ishida, T. Nakajima, Y. Honda, O. Kitao, H. Nakai, T. Vreven, J. A. Montgomery Jr., J. E. Peralta, F. Ogliaro, M. Bearpark, J. J. Heyd, E. Brothers, K. N. Kudin, V. N. Staroverov, R. Kobayashi, J. Normand, K. Raghavachari, A. Rendell, J. C. Burant, S. S. Iyengar, J. Tomasi, M. Cossi, N. Rega, J. M. Millam, M. Klene, J. E. Knox, J. B. Cross, V. Bakken, C. Adamo, J. Jaramillo, R. Gomperts, R. E. Stratmann, O. Yazyev, A. J. Austin, R. Cammi, C. Pomelli, J. W. Ochterski, R. L. Martin, K. Morokuma, V. G. Zakrzewski, G. A. Voth, P. Salvador, J. J. Dannenberg, S. Dapprich, A. D. Daniels, Ö. Farkas, J. B. Foresman, J. V. Ortiz, J. Cioslowski and D. J. Fox, *Gaussian 09, Revision D.01*, Gaussian, Inc., Wallingford CT, 2009.

36 T. Bruhn, A. Schaumlöffel, Y. Hemberger and G. Bringmann, *Chirality*, 2013, **25**, 243.